A Simplified Dynamical System for Tropical Cyclone Intensity Prediction

MARK DEMARIA

NOAA/NESDIS, Fort Collins, Colorado

(Manuscript received 27 December 2007, in final form 24 June 2008)

ABSTRACT

A simplified dynamical system for tropical cyclone intensity prediction based on a logistic growth equation (LGE) is developed. The time tendency of the maximum sustained surface winds is proportional to the sum of two terms: a growth term and a term that limits the maximum wind to an upper bound. The maximum wind evolution over land is determined by an empirical inland wind decay formula. The LGE contains four free parameters, which are the time-dependent growth rate and maximum potential intensity (MPI), and two constants that determine how quickly the intensity relaxes toward the MPI. The MPI is estimated from an empirical formula as a function of sea surface temperature and storm translational speed. The adjoint of the LGE provides a method for finding the other three free parameters to make the predictions as close as possible to the National Hurricane Center best-track intensities. The growth rate is assumed to be a linear function of the vertical shear (S), a convective instability parameter (C) determined from an entraining plume, and their product, where both S and C use global model fields as input. This assumption reduces the parameter estimation problem to the selection of six constants. Results show that the LGE optimized for the full life cycle of individual storms can very accurately simulate the intensity variations out to as long as 15 days. For intensity prediction, single values of the six constants are found by fitting the model to more than 2400 Atlantic forecasts from 2001 to 2006. Results show that the observed intensity variations can be fit more accurately with the LGE than with the linear Statistical Hurricane Intensity Prediction Scheme (SHIPS) formulation, and with a much smaller number of constants. Results also show that LGE model solution (and some properties of real storms) can be explained by the evolution in the two-dimensional S–C phase space. Forecast and other applications of the LGE model are discussed.

1. Introduction

Tropical cyclone (TC) track forecast errors have decreased considerably over the past several decades. However, there have been only modest intensity forecast improvements (DeMaria et al. 2007). Because of the complex physical processes affecting intensity changes, statistical forecast models have remained competitive with much more general prediction systems. For this reason, the National Hurricane Center (NHC) continues to run a hierarchy of operational intensity models that range from the simple Statistical Hurricane Intensity Prediction Scheme (SHIPS; DeMaria et al. 2005) to the fully coupled atmosphere–ocean Hurricane Weather Research and Forecast (HWRF) system (Surgi et al. 2008). The HWRF model became operational in 2007, and is the follow on to the National Centers for Environmental Prediction (NCEP) version of the Geophysical Fluid Dynamics Laboratory (GFDL) coupled hurricane model (Bender et al. 2007).

Several experimental intensity prediction systems of intermediate complexity have also been proposed. Emanuel et al. (2004) showed that a three-layer axisymmetric model coupled with a simplified ocean model can simulate many aspects of TC intensity changes when a parameterization for entrainment as a function of environmental vertical shear is included. Shen (2005) developed an intensity prediction system based on an energetics principal. In Shen's model, the prediction system is reduced to an ordinary differential equation for the integrated TC kinetic energy.

As opposed to the physically based models described above, the SHIPS model is purely empirical. Multiple linear regression is used to relate factors from climatology, persistence, the atmosphere and the ocean to intensity changes. The atmospheric variables are obtained from the NCEP global model and the oceanic

Corresponding author address: Mark DeMaria, NOAA/NESDIS/StAR, 1375 Campus Delivery, CIRA/CSU, Fort Collins, CO 80523.
E-mail: Mark.DeMaria@noaa.gov

DOI: 10.1175/2008MWR2513.1

variables are from sea surface temperature (SST) analyses and satellite altimetry retrievals of ocean heat content (OHC). Predictors from Geostationary Operational Environmental Satellite (GOES) imagery are also included as measures of convective activity. An even simpler statistical model [the Statistical Hurricane Intensity Forecast Model (SHIFOR)] is also run operationally at NHC. SHIFOR only includes predictors from climatology and persistence (Knaff et al. 2003) and is primarily used as a baseline for the evaluation of forecast skill. The experimental Florida State University Super Ensemble (FSSE) is another example of an empirically based TC model. The superensemble methodology optimally combines forecasts from a set of models (Krishnamurti et al. 1999).

Over the past decade, SHIPS has generally been the most skillful of NHC's operational intensity forecast models (DeMaria et al. 2007). Although gradual improvements have been made to SHIPS by including predictors from new data sources such as GOES imagery and satellite altimetry, further improvements may be limited by the underlying linear nature of the model. In the multiple regression formulation, the intensity change over each forecast interval is a linear function of a set of input parameters. However, the intensity change at, say 36–48 h, may depend on the actual intensity at 36 h, but this effect could not be included in the current formulation of SHIPS. Also, a relatively large number of coefficients are needed to represent the intensity evolution. For example, the 2007 version of SHIPS included 21 predictors and separate regression equations for each 6-h forecast interval out to 120 h for a total of 420 coefficients. In this study, a simple dynamical prediction system is introduced that can represent the basic evolution of TCs with a much smaller number of free parameters than SHIPS. Although the prediction system, which is based on a logistic growth equation (LGE), is still empirically based there is a closer relationship to physical processes through a direct inclusion of a maximum potential intensity (MPI) estimate. The LGE formulation bounds the solution between 0 and a fraction of the MPI and allows for a straightforward way to include the effects of land. The complexity of this system lies between the energetics model of Shen (2005) and SHIPS.

The LGE is described in section 2. The MPI estimation method and preliminary real-time forecast results from a version that uses a linear regression approach for the calculation of the model growth rate are presented in section 3. Sections 4 and 5 introduce a new method estimating the parameters of the LGE using the adjoint of the prediction model and a version with a greatly reduced set of predictors. Section 6 tests the adjoint fitting method with the reduced predictor set on individual storms. Section 7 describes how the parameters fitted to a large number of storms can be used to define a two-dimensional phase space (shear and instability) that helps to illustrate the roles of dynamic and thermodynamic factors on intensity changes, and presents results with independent cases. Potential applications of the LGE model are described in section 8.

2. The logistic growth equation

The basic equation for the intensity prediction is based on an analogy with a differential equation commonly used to model population growth. For that application, the LGE can be written as

$$\frac{dP}{dt} = \kappa P - \mu P^2, \tag{1}$$

where P is the species population, t is time, and κ and μ are constants. The first term on the right-hand side represents reproduction, where the growth rate is proportional to the size of the existing population. The second is a mortality term that takes into account available resources and limits growth. This population model was first proposed by the Belgian mathematician P. F. Verhulst in 1838 (Murray 1979). Defining $K = \kappa/\mu$, then (1) becomes

$$\frac{dP}{dt} = \frac{\kappa P(K - P)}{K}. \tag{2}$$

For $P \ll K$, the population growth is exponential. However, as P becomes large the growth rate slows down because of a competition for resources. In the limit as $t \to \infty$ a steady state is reached where $P = K$. The quantity K is called the carrying capacity and represents the maximum population that the environment can support.

For TC intensity prediction, the dependent variable in (1) is replaced by the maximum sustained surface wind V as a function of time. Viewing TC intensification from the point of view of a wind-induced surface heat exchange (WISHE) instability (Emanuel 1986), the surface energy flux depends on the current surface wind speed. Thus, the WISHE process is represented by the reproductive term in (1). The intensification process cannot continue indefinitely and is limited to an upper bound (i.e., the MPI). This process is represented by the second term on the right in (1). The MPI concept was first proposed by Miller (1958), and theoretical formulas have been derived by Holland (1997) and Eman-

uel (1988). Empirical MPI formulas have also been developed from observations (e.g., Whitney and Hobgood 1997). All of these MPI formulas depend on thermodynamic properties of the storm environment.

For intensity prediction a generalized version of (1) is utilized where κ and μ are time dependent and the power of 2 in the second term on the right is replaced with an arbitrary parameter greater than zero. With these assumptions, the intensity evolution is determined from

$$\frac{dV}{dt} = \kappa V - \beta V\left(\frac{V}{V_{\text{mpi}}}\right)^n, \tag{3}$$

where V_{mpi} is the MPI in terms of a maximum surface wind, κ is the time-dependent growth rate, and β and n are positive constants that determine how rapidly and how close the solution for V can come to V_{mpi}. As will be described below, μ in (1) was replaced by $\beta/(V_{\text{mpi}})^n$ to make the steady-state solution to (3) easier to interpret physically.

Similar to the SHIPS model it is assumed that the storm track is known. Then V_{mpi} can be calculated from the SST and atmospheric soundings from model analyses or forecasts of the storm environment. Similarly, κ is assumed to be a function of environmental parameters such as vertical wind shear that can be calculated from analyses or model forecasts. Details of how the four parameters V_{mpi}, κ, β, and n are estimated will be described in sections 3–4.

To better understand the behavior of (3), consider the case where the four parameters are all constants. The analytic solution of (3) with constant coefficients is described by Thieme (2003) in the context of population modeling. For this case, the solution has two families of solutions. When $\kappa < 0$, both terms on the right-hand side are always negative, so V decays to zero. The solution also decays to zero when $\kappa = 0$. When $\kappa > 0$ the first term on the right-hand side dominates when V is small, so V increases exponentially. As V increases, the second term becomes important, and in the limit as $t \to \infty$, a steady-state solution is reached where dV/dt is zero. Defining the steady-state value of V as V_s, setting $dV/dt = 0$ in (3) and solving for $V = V_s$ gives

$$V_s = V_{\text{mpi}}\left(\frac{|\kappa|}{\beta}\right)^{1/n}. \tag{4}$$

The absolute value is included in (4) because V_s can be used as a scale for V, whether κ is positive or negative. Equation (4) shows that in the limit as $n \to \infty$, the steady-state solution approaches V_{mpi}.

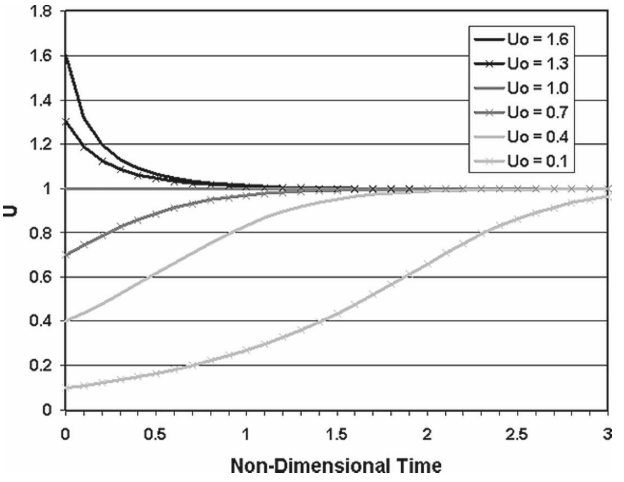

FIG. 1. The analytic solution to the nondimensional form of the logistic growth equation with positive κ and $n = 3$ for several values of the initial condition U_o.

Assuming $\kappa \neq 0$, Eq. (3) can be simplified by defining nondimensional wind speed U and time τ as

$$U = \frac{V}{V_s}, \tag{5}$$

$$\tau = |\kappa| t. \tag{6}$$

Using (4)–(6), (3) can be written as

$$\frac{dU}{d\tau} = U(s - U^n), \tag{7}$$

where s is the sign of κ ($s = 1$ if $\kappa > 0$ or $s = -1$ if $\kappa < 0$). The solution to (7) is given by

$$U(\tau) = U_o e^{s\tau}[1 + sU_o^n(e^{sn\tau} - 1)]^{(-1/n)}, \tag{8}$$

where U_o is the initial value of U.

Figures 1 and 2 show $U(\tau)$ for several values of U_o for $\kappa > 0$ and $\kappa < 0$. The solutions in Figs. 1 and 2 are for $n = 3$. Here U decays to zero with time for negative κ and approaches 1 ($V = V_s$) for positive κ. The effect of the parameter n can be seen in Fig. 3, which shows $U(\tau)$ for positive κ with $n = 1, 2 \ldots 5$. This parameter primarily affects the steepness of the U curve. For the dimensional speed V, n also affects the value of the steady-state solution that is being approached as t increases, as can be seen from (4).

The nondimensional scaling in (5)–(6) is not valid for $\kappa = 0$. For this case, the analytic solution of (3) is given by

$$V(t) = V_o\left[1 + \beta n t\left(\frac{V_o}{V_{\text{mpi}}}\right)^n\right]^{(-1/n)}, \tag{9}$$

where V_o is the initial value of V. Equation (9) shows that the V decays slowly to zero when $\kappa = 0$.

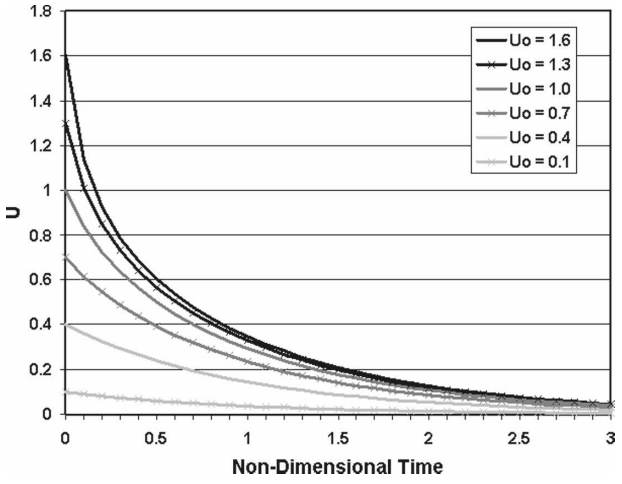

FIG. 2. As in Fig. 1, but for negative κ.

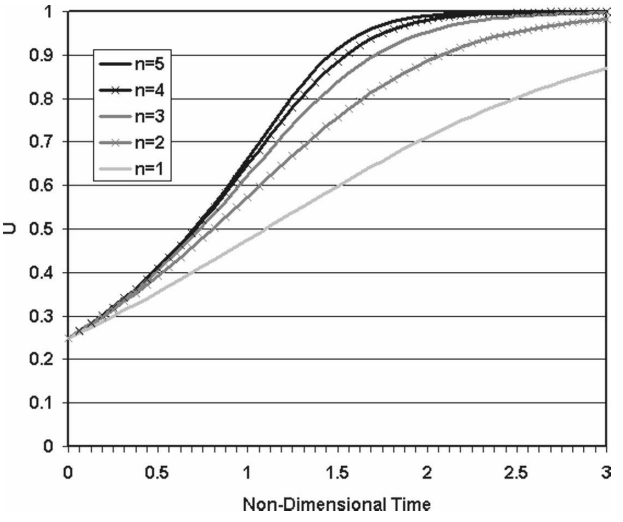

FIG. 3. The analytic solution to the nondimensional form of the logistic growth equation with $U_o = 0.25$ for several values of n.

The LGE model formulation is closely related to a nonlinear statistical method called logistic regression (Wilks 2006). Logistic regression is usually employed in problems where the predicted variable is bounded between 0 and 1. In fact, the most common functional form used in logistic regression is mathematically equivalent to (8) for the case with $n = s = 1$. However, when applied to the forecast problem, V_{mpi} and κ are time dependent so it more straightforward to use the differential form in (3) and integrate it numerically, rather than fit a series of the analytic solutions over short time segments. From this point of view the LGE model can be thought of as a differential or local form of logistic regression.

Equation (3) is valid for the case where the storm center is over water. When the storm center is over land, the empirical inland wind decay model described by Kaplan and DeMaria (1995) is utilized. The maximum wind is reduced by a factor of R when the storm first moves over land to account for differences in surface roughness. If the storm moves back over the water, V is divided by R. For the remaining time over land, the storm decays toward a background wind V_b with an e-folding time given by α^{-1}. Thus, the inland wind model is determined from the three specified parameters R, V_b, and α. Kaplan and DeMaria (2001) developed a second set of parameters for higher-latitude storms. The low-latitude values are used when the storm center is south of 36°N, the high-latitude values are used when it is north of 40°N, and linear interpolation is used in between. At all latitudes $R = 0.9$, so only α and V_b are linearly interpolated.

DeMaria et al. (2006) showed that the inland wind model has a low bias for storms that move over islands and narrow landmasses, which can be corrected by multiplying α by the fraction of the storm area over land (F), where the storm area is defined as a circle with a radius of 111 km. With these assumptions, the evolution of V when the storm is over land is determined from

$$\frac{dV}{dt} = -\alpha(V - V_b), \tag{10}$$

where α includes the fractional area correction F. Because of the factor F and the linear interpolation as a function of latitude, both α and V_b are specified functions of time. Equations (3) and (10) will be referred to as the logistic growth equation model (LGEM).

3. Preliminary forecast results

A preliminary version of LGEM was developing using a multiple regression technique (hereafter LGEM-MR) for estimating the model parameters from the SHIPS model input. This input included maximum winds and storm positions at 6-h intervals from the NHC best track (Jarvinen et al. 1984) and predictors from Reynolds SST (Reynolds et al. 2002) and the NCEP Global Forecasting System (GFS) model analyses (Yang et al. 2006). LGEM-MR was run in real time at NHC during the Atlantic and eastern North Pacific 2006 and 2007 hurricane seasons. The developmental sample included 1982–2005 for the 2006 version and 1982–2006 for the 2007 version. The results from these preliminary tests are presented here since a direct comparison with the operational SHIPS model is possible and to provide motivation for the more general parameter estimation method described in sections 4 and 5.

For storms over land, all the LGEM parameters (R, α, and V_b) are known from the inland wind model. For storms over water, κ and $V_{\rm mpi}$ as a function of time and the constants n and β in (3) need to be determined. The $V_{\rm mpi}$ was calculated as a function of the SST along the storm track using the empirical formulas developed by DeMaria and Kaplan (1994) for the Atlantic and Whitney and Hobgood (1997) for the eastern North Pacific. These formulas were developed in a storm-relative coordination system, so a fraction of the storm translational speed is added to the $V_{\rm mpi}$ estimate using the equation developed by Schwerdt et al. (1979).

To calculate κ, n, and β, (3) was solved for κ to give

$$\kappa = \left(\frac{1}{V}\right)\frac{dV}{dt} + \beta\left(\frac{V}{V_{\rm mpi}}\right)^n, \qquad (11)$$

where dV/dt was determined from the best-track intensities using a 24-h centered time difference. Only those cases where the storm was over water for each 24-h period are included. Initial guesses were made for the constants β and n, and the best tracks were divided into a sequence of 5-day forecasts in the same way as for the SHIPS model. With the above assumptions, (11) was used to calculate "observed" values of κ for each of the 5-day forecasts. Then, regression equations were developed for the estimation of κ using the SHIPS predictors, but without those from satellite data or the quadratic terms (see DeMaria et al. 2005). The satellite data were excluded because they are not available for the entire SHIPS developmental sample. The quadratic terms were not needed because they generally help to constrain the intensity changes in SHIPS for the stronger storms, but the LGE automatically bounds the solution. The regression procedure was repeated with several values of β and n and those that maximized the variance explained in the linear prediction of κ were determined. The final values of β and n were 1/24 h^{-1} and 2.5, respectively. Persistence was included in the regression by calculating κ at the beginning of each forecast from the intensity values from the previous 12 h, which was used as a predictor for κ at each forecast time. A separate set of regression equations was used to predict κ every 6 h from 0 to 120 h.

Whether over land or water, LGEM contains exponentially growing or decaying solutions so that a forward-time-differencing scheme can be used for the numerical solution of (3) or (10) provided that the time step is smaller than $2/\alpha_{\rm max}$, where $\alpha_{\rm max}$ is the largest value of the decay or growth coefficient. In LGEM, the largest coefficient is in the inland decay model, where $\alpha_{\rm max} \sim 10\ h^{-1}$, which requires a time step less than ~20 h. Since LGEM is computationally trivial a time step of 1 h was used, which was found to be more than adequate for stability and accuracy of the solution and includes all of the 6-hourly best-track data points. The 6-hourly values of κ and $V_{\rm mpi}$ were linearly interpolated to provide hourly values for the time integration.

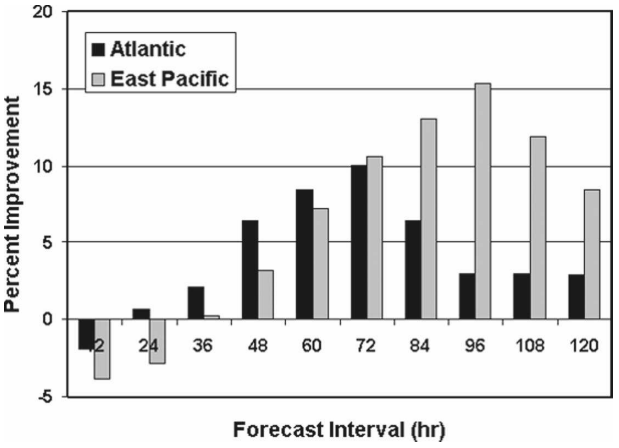

FIG. 4. The improvement of the real-time Atlantic and east Pacific LGEM intensity forecasts relative to the operational SHIPS forecasts for the combined 2006–07 season samples.

The real-time LGEM-MR runs used the same input as the operational SHIPS model, including the NHC operational forecast track and predictors estimated from GFS forecast fields, rather than the GFS analyses used to develop the regression equations. Figure 4 shows the percent improvement of the LGEM-MR forecasts relative to the SHIPS forecasts for the 2006–07 sample. The LGEM-MR errors were larger than those of SHIPS at the early forecast periods, but were up to 17% smaller at the longer times in the east Pacific. In the Atlantic, the LGEM-MR errors were up to 10% smaller than those of SHIPS. Using a method that accounts for serial correlation of the forecasts (Franklin and DeMaria 1992), the SHIPS – LGEM-MR error differences in Fig. 4 were statistically significant at the 95% level at 60–72 h in the Atlantic and at 72–96 h in the east Pacific. These results indicate that the LGE formulation provides improvement relative to the linear regression used in the SHIPS. Based on this success, LGEM-MR will continue to be run in real time.

Although LGEM-MR shows promise, it has some shortcomings. First, the short-term intensity forecasts errors were larger than those from SHIPS. This may be due to the fact that the κ error is being minimized by the multiple regression, rather than the predicted maximum wind. Also, the number of coefficients is almost as large as for SHIPS. In the next two sections a more general method for estimating the LGE parameters and

a strategy for reducing the numbers of predictors are described.

4. Generalized parameter estimation

As described above for LGEM-MR, V_{mpi} is specified along the storm track, so the remaining parameters in (3) that need to be specified are κ as a function of time and the constants β and n. It will again be assumed that κ is a linear function of large-scale variables such as vertical shear, which are known functions of time. Letting these large-scale variables be represented by x_i for $i = 1, 2, \ldots I$ then κ is given by

$$\kappa(t) = a_1 x_1(t) + a_2 x_2(t) + \ldots a_I x_I(t) + b, \qquad (12)$$

and the parameter estimation problem is reduced to the determination of the $I + 3$ constants β, n, a_i, and b.

An elegant method for estimating model parameters for dynamical systems has been developed as part of data assimilation systems (Errico 1997). For example, Zhu and Navon (1999) showed that the adjoint of a global forecast model can be used to optimize diffusion and boundary layer flux parameters. As described above, in the general case with time-dependent parameters, (3) or (10) must be solved numerically. The numerical solution is described first, followed by the adjoint of the discretized system and its application to parameter estimation.

Letting t be discretized using

$$t_m = m\Delta t, \quad m = 0, 1, 2, \ldots, M \qquad (13)$$

and any variable with a subscript m be evaluated at t_m, then the forward-difference form of the combined Eqs. (3) and (10) can be written as

$$V_{m+1} = R_m V_m + \left\{ \delta_m \left[\kappa_m R_m V_m - \beta \left(\frac{R_m V_m}{V_{\mathrm{mpi},m}} \right)^n R_m V_m \right] - \varepsilon_m [\alpha_m (R_m V_m - V_{b,m})] \right\} \Delta t. \qquad (14)$$

Although more accurate time-difference methods are available, forward differencing simplifies the derivation of the adjoint equation and accuracy can be ensured by making the time step as small as needed, as described in section 3. In (14), $\delta_m = 1$ if the storm center is over water at time t_m and $\delta_m = 0$ if the storm is over land, and vice versa for ε_m. The R_m factor takes into account the reduction in wind speed when the storm first moves from water to land and the increase when it moves back over the water, which is part of the inland wind model. Mathematically, $R_m = R$ for the first time step over land, $R_m = 1/R$ for the first time step over water and $R_m = 1$ for all other time steps. Given the initial condition $V = V_o$, (14) can be used to find V_m for $m = 1, 2, \ldots M$ and will be referred to as the forward model.

The model coefficients will be chosen so that the solution of the forward model is as close to the observed intensity values as possible. The observations are the maximum sustained surface winds from the NHC best track, which are available at 6-h intervals. The best-track intensity estimates were linearly interpolated to the 1-h time step of the forward model and are denoted by O_m. Because the best-track intensities are reported in knots rounded to the nearest 5, units of knots are used for V_m and O_m. For a model integration of length t_M, the model error E is defined as

$$E = \frac{1}{2} \sum_{m=1}^{m=M} (V_m - O_m)^2. \qquad (15)$$

If the gradient of E with respect to the constants β, n, a_i, and b could be determined, the optimal values could be found using a gradient descent algorithm. This is accomplished using the method of Lagrange multipliers where the forward model equations are appended to E as constraints. Letting (14) be represented symbolically by

$$V_m = R_{m-1} V_{m-1} + G_{m-1} \Delta t, \qquad (16)$$

then the Lagrange function J can be written as

$$J = E + \sum_{m=1}^{m=M} \lambda_m [V_m - (R_{m-1} V_{m-1} + G_{m-1} \Delta t)], \qquad (17)$$

where λ_m are Lagrange multipliers. Setting the derivative of J with respect to V_m to zero gives the following adjoint model:

$$\lambda_M = -(V_M - O_M), \qquad (18)$$

$$\lambda_m = \lambda_{m+1} \left\{ R_m + \delta_m \Delta t R_m \left[\kappa_m - \beta (n+1) \left(\frac{R_m V_m}{V_{\mathrm{mpi},m}} \right)^n \right] - \varepsilon_m \alpha_m R_m \Delta t \right\} - (V_m - O_m). \qquad (19)$$

Note that the adjoint equation in (19) is integrated backward in time to give λ_m for $m = M - 1, M - 2, \ldots, 1$ after being initialized with (18).

Using the discretized version of (12), the gradients of J with respect to β, n, a_i, and b are given by

$$\frac{\partial J}{\partial \beta} = \sum_{m=1}^{m=M} \lambda_m \delta_{m-1} \Delta t \left(\frac{R_{m-1} V_{m-1}}{V_{\mathrm{mpi},m-1}} \right)^n R_{m-1} V_{m-1}, \tag{20}$$

$$\frac{\partial J}{\partial n} = \sum_{m=1}^{m=M} \lambda_m \delta_{m-1} \Delta t \beta \left(\frac{R_{m-1} V_{m-1}}{V_{\mathrm{mpi},m-1}} \right)^n \ln\left(\frac{R_{m-1} V_{m-1}}{V_{\mathrm{mpi},m-1}} \right) R_{m-1} V_{m-1}, \tag{21}$$

$$\frac{\partial J}{\partial a_i} = -\sum_{m=1}^{m=M} \lambda_m \delta_{m-1} \Delta t R_{m-1} (x_{i,m-1} V_{m-1}), \tag{22}$$

$$\frac{\partial J}{\partial b} = -\sum_{m=1}^{m=M} \lambda_m \delta_{m-1} \Delta t R_{m-1} (V_{m-1}), \tag{23}$$

and are used to find the $I + 3$ constants that minimize the error in the forward model as part of a steepest descent algorithm. Although more general minimization algorithms are available, the steepest descent algorithm performed quite well (as will be demonstrated in section 6) provided that the components of the gradient were scaled by typical values of the $I + 3$ constants to account for their differing units.

5. Reduced predictor set

As described in section 3, LGEM-MR used most of the predictors in the SHIPS model and a separate set of regression equations for κ was developed at each time interval. The separate regressions were needed because of the inclusion of persistence, which is the value of κ based on the intensity change from $t = -12$ to $t = 0$ h. The influence of that predictor decreases at the longer forecast times. As will be described in section 8, the adjoint formulation provides an alternate method for including the known storm evolution up to the forecast time, so separate versions of (12) at each forecast period are not needed.

Besides persistence, most of the SHIPS predictors are related to either the dynamic or thermodynamic properties of the storm environment (DeMaria et al. 2005). The most important dynamical property is the vertical shear, which is the magnitude of the 850–200-hPa vector wind difference, where the winds at 850 and 200 hPa are averaged over a circular area centered on the storm with a radius of 500 km. The thermodynamic properties are measured by a number of predictors in SHIPS including the 200-hPa temperature, midlevel relative humidity, and a parameter that measures the equivalent potential temperature difference between an undilute parcel lifted from the surface and that of the parcel environment. These thermodynamic predictors can be replaced by a single variable obtained from an entraining plume model, as described below.

As summarized by Zipser (2003), instability indices such as convective available potential energy (CAPE) or lifted index (LI), which have been used in the midlatitudes are not appropriate for the tropics because some of the neglected factors such as the weight of the condensate and entrainment are of first-order importance. For this reason, an entraining plume model (Simpson and Wiggert 1969) is used to measure convective instability.

The plume model uses temperature and moisture soundings from the GFS analyses averaged over an annulus from 200 to 800 km from the storm center and the Reynolds SST for the surface temperature. The plume is initialized with a surface-based parcel with an upward vertical velocity of 8 m s^{-1}. This fairly large value was chosen so that the parcel would reach its lifting condensation level for most soundings. The evolution of the parcel is determined by the thermodynamic formulation of Ooyama (1990), where the ice phase is included by considering a single moisture variable that behaves like water for temperatures above 0°C and like ice below 0°C. Entrainment is included by assuming that the mass entrainment rate is inversely proportional to the radius of the parcel (Simpson and Wiggert 1969), so that

$$\left(\frac{1}{M} \right) \frac{dM}{dz} = \frac{C_E}{r}, \tag{24}$$

where M is the parcel mass, z is height, r is the parcel radius, and C_E is the entrainment rate (specified to be 0.1). The initial parcel radius is 0.5 km, which is a rea-

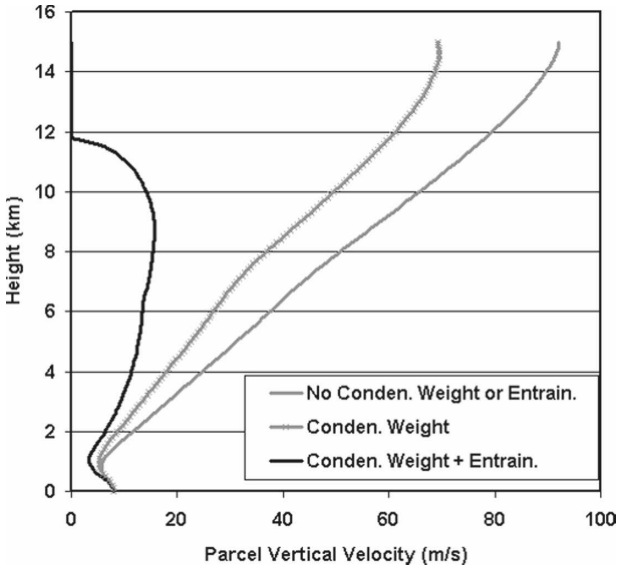

FIG. 5. The vertical velocity as a function of height from the entraining plume model. The temperature and moisture profiles of the parcel environment are from a mean Atlantic hurricane sounding. Three versions of the model were run where both entrainment and condensate weight were neglected, entrainment was neglected, and both entrainment and condensate weight were included.

sonable value for tropical convection (LeMone and Zipser 1980). The calculation includes the weight of the condensate and virtual temperature effects on the buoyancy. Precipitation was included by assuming that the rate of fallout of the condensate from the parcel is proportional to the amount of condensate present, with a proportionality constant of 600^{-1} s^{-1}.

Figure 5 shows vertical velocity profiles from the plume model for a mean Atlantic tropical sounding (J. Dunion 2008, personal communication). The sounding is a composite from Caribbean stations that were determined to be uninfluenced by the stable Saharan air layer (SAL). The effects of condensate weight and entrainment can be seen by comparing the three profiles in Fig. 5. Without these two effects, the vertical velocities are unrealistically large. With both effects included, the vertical velocities are on the high side but within the range of what has been observed in tropical convection (Zipser 2003).

For the reduced predictor set, dynamical effects are included through the 850–200-hPa vertical shear (S) and thermodynamic effects are include through the predictor (C), which is the z = 0–15-km average of the vertical velocity of the parcel in the plume model. With these assumptions (12) becomes

$$\kappa = a_1 S + a_2 C + a_3 SC + b. \qquad (25)$$

The a_3 term is included in (25) to allow for interactions between the vertical shear and convective instability. With the reduced predictor set the parameter estimation problem is reduced to finding the six constants β, n, a_1, a_2, a_3, and b that minimize the LGEM intensity solution error.

6. Simulation of individual storms

As a first test of the generalized parameter estimation, LGEM simulations of the entire life cycles of individual storms were considered. These simulations evaluate how well the mathematical representation described in section 2 and the assumed form of κ in (25) can fit the observations for the case when the track, SST, S, and C are accurately estimated. For these simulations, SST, S, and C are determined along the observed storm track using the Reynolds SST and GFS analyses. The predictors S and C are normalized by subtracting their sample means and dividing by the standard deviations so that a_i and b in (25) have the same units as κ, and b represents the mean value of κ.

The first test case is Hurricane Frances (2004), which formed west of the Cape Verde Islands at 0000 UTC 25 August, intensified to a category four hurricane over the mid-Atlantic, and weakened to a category 2 storm before striking southeast Florida north of Palm Beach (Beven 2004). Frances weakened to a tropical storm as it crossed Florida, briefly reentered the Gulf of Mexico, but did not regain hurricane intensity. Frances made a second landfall in the Big Bend region of northwest Florida and transitioned to an extratropical cyclone over West Virginia. LGEM was initialized at 0000 UTC 25 August with an intensity of 25 kt and was run until just before the extratropical transition at 1800 UTC 8 September (14.75 days).

The steepest descent algorithm converged after a few hundred iterations and the mean absolute error (MAE) of the intensity prediction over the 14.75-day forecast period was reduced to a surprisingly low 3.9 kt. Figure 6 shows the maximum wind from the LGEM simulation, the NHC best track, and the MPI. This figure shows that the fitted LGEM reproduces nearly every aspect of the intensity variation of Frances. The largest error occurs near 280 h where the inland wind model predicted too much decay as the storm crossed Florida. However, the difference between the LGEM prediction and the best track is less than about 10 kt for the rest of the integration.

Additional tests of the parameter estimation were performed for long-lived storms from 2001 to 2006. The 13 cases are listed in Table 1, which were selected to include storms over different parts of the Atlantic basin

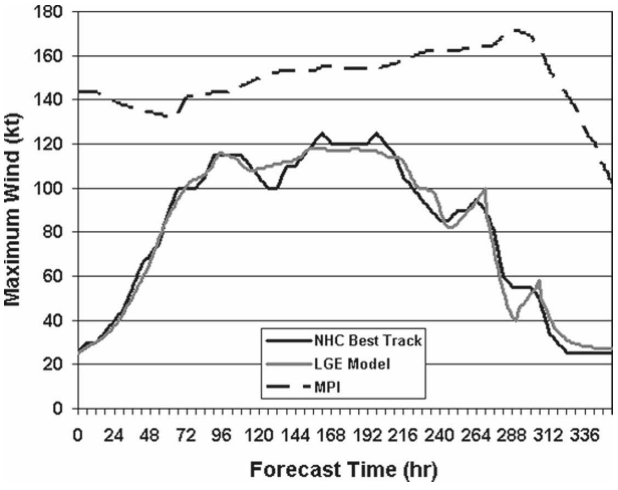

FIG. 6. The 14.75-day LGEM forecast of the intensity of Hurricane Frances (2004) and the corresponding NHC best-track intensity. The MPI estimated from the SST is also shown.

and different times during the hurricane season. Table 1 also shows the values of the six constants that minimize the LGEM simulation for each storm and the MAE. Table 1 shows that the MAE was reduced to between 2.8 and 10.6 kt, with a 13-storm-average MAE of 6.0 kt. This result provides justification for the functional form assumed in LGEM since 6 kt is close to the noise level of the NHC best-track intensities, which are rounded to the nearest 5 kt.

Table 1 shows the values of the six constants for each storm fit, and the 13-storm average. Although there is variability in the coefficients, there is also some consistency. The 13-storm-average coefficients show that the growth rate κ decreases with S and increases with C as expected from a physical basis. The average value of a_3 is positive, which can be interpreted as a modification of the impact of shear by convection. When C is large, this term will partially cancel the a_1 term, reducing the impact of the vertical shear.

In many cases the deviation of the fitted LGEM simulation from the NHC best track can be related to storm characteristics not included in the model. As an example, Fig. 7 shows the fitted LGEM solution and best track for Hurricane Katrina. The LGEM simulation is generally too high from about 84 to 96 h. The observed intensity stayed fairly constant during this period as the storm went through an eyewall replacement cycle (Knabb et al. 2005). The intensity changes during this period were determined by inner-core processes, rather than the large-scale processes included in LGEM. From about 100 to 120 h, Katrina rapidly intensified to 150 kt and the LGEM prediction underestimated the maximum wind. The storm moved over a warm ocean eddy during this period (Mainelli et al. 2008), which was not represented in the model since the SST was fairly constant during this period.

7. Multiple storm parameter estimation

To use LGEM in a predictive mode rather than for simulations as in section 6, a single set of the six constants needs to be determined from training data and

TABLE 1. Values of the LGE model parameters for 13 Atlantic storms from the 2001–06 seasons and the mean absolute error of the intensity simulation. The starting time–date, LGE model integration length, and peak intensity of the each storm from the NHC best track are also shown. The values for a simultaneous fit of the LGE model to all Atlantic storms from 2001 to 2006 are also listed.

Name	Yr	Time–start date	Length (h)	Peak intensity (kt)	n	β (h^{-1})	b (h^{-1})	a_1 (h^{-1})	a_2 (h^{-1})	a_3 (h^{-1})	MAE (kt)
Felix	2001	0600 UTC 10 Sep	8.75	100	2.1	0.0224	0.0179	0.0074	0.0098	0.0248	3.5
Olga	2001	0000 UTC 24 Nov	10.75	80	1.3	0.0377	0.0130	−0.0117	0.0071	0.0006	3.0
Isidore	2002	1200 UTC 17 Sep	10.00	110	3.3	0.0263	0.0132	−0.0021	0.0017	0.0026	5.1
Kyle	2002	1800 UTC 20 Sep	21.75	75	2.1	0.0548	0.0492	−0.0105	0.0015	0.0003	7.6
Claudette	2003	1800 UTC 8 Jul	8.25	75	1.7	0.0630	0.0160	−0.0125	−0.0146	0.0144	4.5
Isabel	2003	0000 UTC 6 Sep	13.25	145	2.4	0.0580	0.0336	−0.0180	0.0096	0.0108	9.4
Frances	2004	0000 UTC 25 Aug	14.75	125	2.5	0.0416	0.0189	−0.0068	0.0013	0.0055	3.9
Ivan	2004	1800 UTC 2 Sep	15.75	145	2.6	0.0212	0.0129	−0.0032	0.0049	0.0020	10.6
Katrina	2005	1800 UTC 23 Aug	7.00	150	2.9	0.0634	0.0285	0.0078	−0.0123	0.0000	6.6
Wilma	2005	1800 UTC 15 Oct	10.00	160	4.8	0.0408	0.0151	−0.0064	0.0007	−0.0044	10.2
Epsilon	2005	1200 UTC 29 Nov	9.25	75	2.5	0.0010	0.0079	0.0029	0.0125	0.0149	5.0
Ernesto	2006	1800 UTC 24 Aug	7.75	65	2.8	0.0448	0.0083	0.0053	0.0164	−0.0182	2.8
Helene	2006	1200 UTC 12 Sep	12.00	105	2.5	0.0548	0.0166	−0.0018	−0.0043	0.0030	6.1
13-storm avg	—	—	11.50	108	2.6	0.0408	0.0159	−0.0030	0.0026	0.0043	6.0
2001–06 sample	—	—	4.0	76	2.6	0.0256	0.0063	−0.0085	0.0005	−0.0041	11.1
2001–05 sample	—	—	4.0	77	2.6	0.0253	0.0065	−0.0087	0.0007	−0.0040	11.1

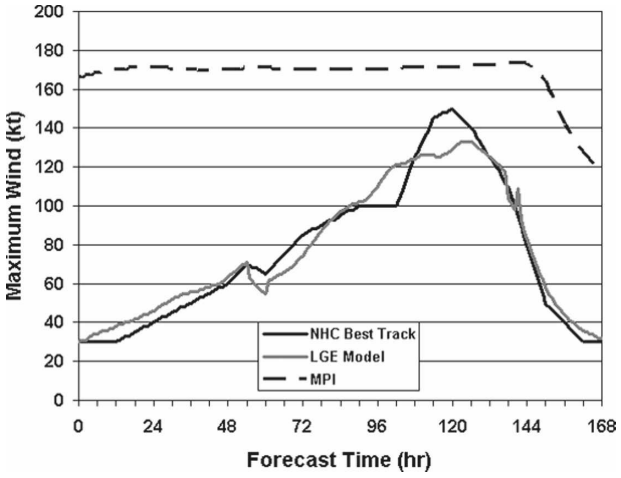

FIG. 7. As in Fig. 6, but for the 7-day LGEM forecast of the intensity of Hurricane Katrina (2005) .

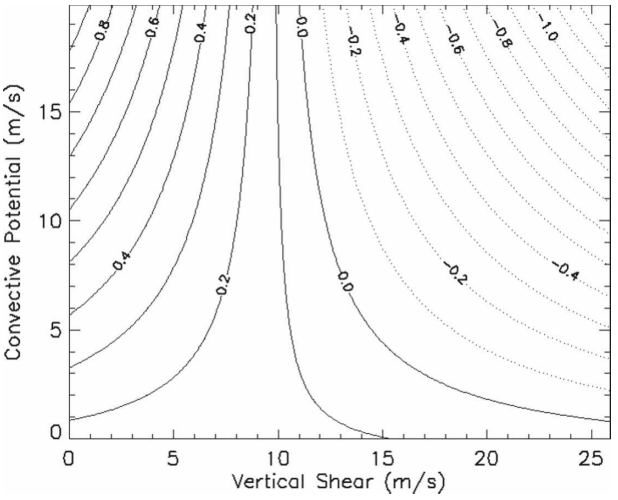

FIG. 8. The growth rate κ as a function of S and C.

then used on new storms. For this purpose, the model was simultaneously fitted to all of the Atlantic storm cases from 2001 to 2006. The cases before 2001 used to develop LGEM-MR described in section 3 were excluded because the SHIPS developmental sample uses operational GFS analyses since 2001, but NCEP reanalysis fields before 2001. The NCEP reanalysis moisture fields had a low-level dry bias relative to the operational analyses, which made the C predictor inconsistent before and after 2001.

To better represent how the model would be used in real time, each storm case was divided into a sequence of 5-day forecasts. For example, if a particular storm lasted for 6 days (144 h), it was divided into 24 forecasts from 0 to 120, 6 to 126, . . . 138 to 144 h. The first 5 cases are 120-h predictions, the next is 114 h and the last is 6 h. The 2001–06 sample includes 2465 forecast cases at 6 h, decreasing to 836 cases at 120 h.

Similar to the individual storm fits, S and C are normalized by subtracting the sample mean and dividing by the standard deviation. For the 2001–06 sample, the mean and standard deviation are 9.0 and 5.6 m s^{-1} for S and 7.5 and 4.1 ms^{-1} for C.

The values of β, n, a_1, a_2, a_3, and b that minimize the forward model error for the 2465 forecasts from 2001 to 2006 are shown at the bottom of Table 1. The value of n for the 2001–06 sample is the same as that from the average of the 13 individual storm fits, and the signs of all the other constants are the same, except for a_3. As will be described below, the negative value of this coefficient for 2001–06 is related to storms that are undergoing extratropical transition. Using the 2001–06 values in Table 1 for β and n and the value of b for the average value of κ, the steady solution defined by (4) is only about 58% of the MPI. This result is consistent with DeMaria and Kaplan (1994) and Emanuel (2000) who showed that TCs rarely reach their MPI.

The roles of dynamic and thermodynamic factors on the LGEM intensity changes can be seen by considering κ as a function of S and C using the 2001–06 fit. Figure 8 shows contours of κ, where S and C range from zero to the mean plus three standard deviations. For S less than about 12 m s^{-1}, κ increases with C and decreases with S. Over most of this region the influence of S is more important than C since the contours are almost vertical. For low values of C, the influence of S decreases. Physically, this result suggests that as long as there is some potential for convection, the primary influence on TC intensification is the vertical shear. For very large values of shear, κ becomes negative, indicating dissipation. For large values of shear, the relationship between C and κ is reversed. This is probably due to the influence of higher-latitude storms that are beginning to take on extratropical characteristics. For these storms, the C values tend to be low, but the S values are high. The growth rate is less negative or slightly positive for these types of storms.

Equation (4) can be written as

$$\frac{V_s}{V_{\mathrm{mpi}}} = \left(\frac{|\kappa|}{\beta}\right)^{1/n}. \tag{26}$$

Using the 2001–06 coefficients from Table 1, (26) and (25) can be used to calculate the ratio of the steady-state solution to the SST-based MPI estimate as a function of S and C. This ratio can be interpreted as an MPI adjustment factor (MAF) that takes into account shear and convective instability. Figure 9 shows that for very low S and high C, the MAF is close to 1. As expected,

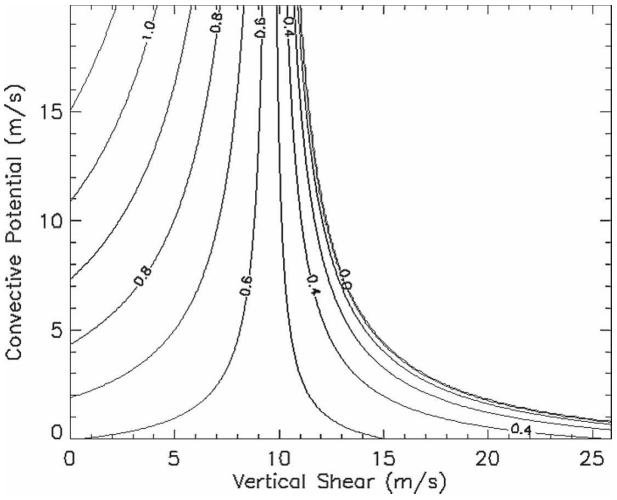

FIG. 9. The MPI adjustment factor as a function of *S* and *C*.

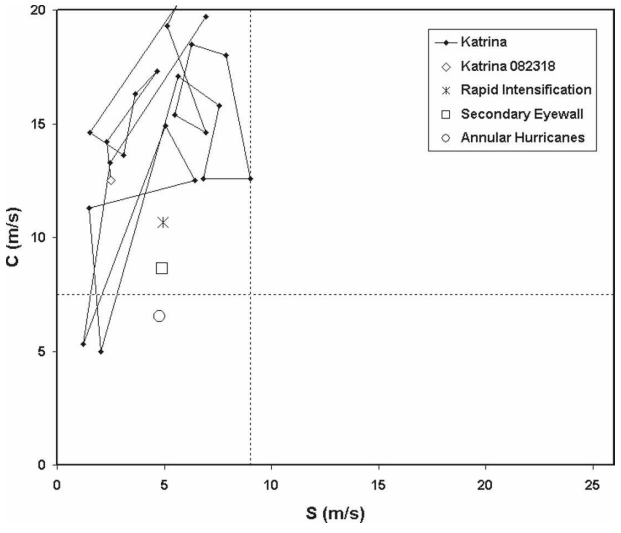

FIG. 10. The time evolution of *S* and *C* for Hurricane Katrina (2005) from its initial formation to just before its Gulf Coast landfall. The average *S*–*C* values for all rapidly intensifying TCs, storm with secondary eyewall formation, and annular hurricanes from the 2001–06 sample are also shown. The dashed lines are the sample mean values of *C* and *S*.

the MAF decreases to zero as the shear becomes large, and there is greater sensitivity to *S* than *C*. The effect of shear on the MPI in Fig. 9 is qualitatively similar to that described by Zeng et al. (2008). The reversal of the effect of *C* on MAF for large values of *S* is again due to storms beginning extratropical transition.

Figures 8 and 9 show that the location in the *S*–*C* plane determines the storm intensity evolution in LGEM. Thus, it is instructive to consider the *S*–*C* trajectory of storms as they evolve. Figure 10 shows the *S*–*C* evolution for Hurricane Katrina from its initial formation on 23 August until just before its Gulf Coast landfall on 29 August. The storm spent nearly its entire lifetime in the upper-left quadrant of the diagram, which indicates that the shear was below average and the convective potential was above average. Katrina underwent at least one eyewall replacement cycle and also rapidly intensified.

Figure 10 also shows the average *S* and *C* values for the 108 cases that rapidly intensified (RI), the 31 cases that had secondary eyewall formation (SEF), and the 20 cases that were identified as annular hurricanes (AH). Rapid intensification cases are those where the maximum winds increased by 30 kt or more in the following 24 h (Kaplan and DeMaria 2003), the SEF cases were identified from microwave imagery (J. Kossin and M. Sitkowski 2008, personal communication), and the annular hurricanes are fairly steady-state storms with large eyes and few rainbands as determined by Knaff et al. (2008). The RI and SEF points are located in the upper-left quadrant, similar to Katrina. However, the AH point is in the lower-left quadrant. This result indicates that low vertical shear is important for all three types of storms, but the convective instability helps to distinguish between RI–SEF behavior and AH behavior.

Figure 11 shows the *S*–*C* evolution for Hurricane Claudette (2003) from its formation on 8 July until just before its landfall in Texas on 15 July. Claudette transformed from a wave into a tropical storm in the Central Caribbean and briefly became a category 1 hurricane after about 2 days before weakening to a tropical storm due to interaction with strong vertical shear (Beven

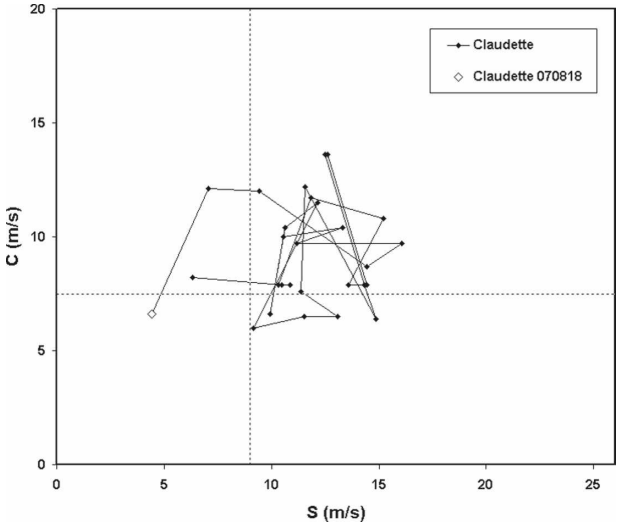

FIG. 11. The time evolution of *S* and *C* for Hurricane Claudette (2003) from its initial formation to just before its Texas coast landfall. The dashed lines are the sample mean values of *C* and *S*.

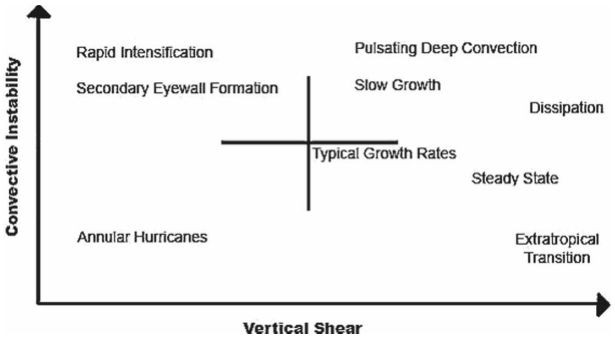

FIG. 12. A conceptual diagram illustrating the use of the *S–C* phase space to anticipate tropical cyclone behavior.

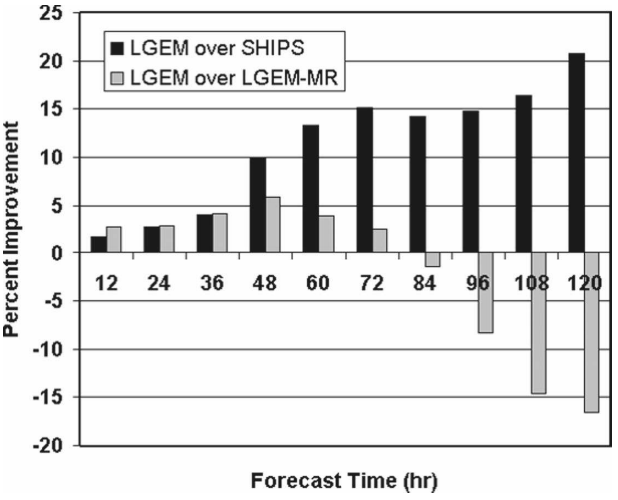

FIG. 13. The percent improvement of the LGEM intensity forecasts over SHIPS and SHIPS-MR for independent cases from the 2006–07 Atlantic hurricane seasons. All forecasts used "perfect-prog" input.

2003). The storm moved into the Gulf of Mexico and remained a tropical storm until just before its landfall along the central Texas coast when it again strengthened to a category 1 hurricane. The storm was in the upper-right quadrant of the *S–C* diagram for most of its lifetime with *S* values near 12 m s^{-1} and *C* values near 10 m s^{-1}. In this quadrant the favorable convective instability is balanced by unfavorable shear. Figure 8 shows that for these values of *S* and *C*, κ is small but positive. Infrared satellite imagery for Claudette (not shown) indicated that Claudette maintained deep convection, but it was asymmetric and highly transient. This result suggests that storms in this part of the phase space have a very unsteady behavior and do not intensity rapidly. Just before landfall Claudette moved into the upper-left quadrant of the *S–C* phase space, which is consistent with its reintensification to a hurricane.

The above results suggest that monitoring the *S–C* evolution might be useful for anticipating TC behavior. Figure 12 shows a conceptual diagram further illustrating this idea. The various behaviors would not be represented by single points in a diagram like Fig. 12, but as probability distributions in the *S–C* plane that could be determined from large samples of various types of storms. The locations of the maximum probabilities could also be determined as were shown for the RI, SEF, and AH cases in Fig. 10.

The results in section 3 showed that LGEM-MR improved on the SHIPS forecasts at most times for real-time runs from the 2006 to 2007 seasons. These cases were with fully independent data and operational input. As a test of LGEM with the reduced predictor set, the Atlantic cases from 2006 to 2007 are again used. The 2007 LGEM runs used the six coefficients in Table 1 from the 2001 to 2006 sample, and the 2006 runs used the coefficients from the 2001 to 2005 sample, which are also shown in Table 1. The coefficients from the sample without 2006 are very similar to those with 2006, suggesting that the model fit is fairly robust. For comparison with LGEM, the 2007 version of the operational SHIPS model and LGEM-MR were run on these same cases. Similar to LGEM, the SHIPS and LGEM-MR models for the 2007 (2006) forecasts were developed from data through 2006 (2005). The combined 2006–07 sample includes 390 forecast cases at 12 h decreasing to 102 cases at 120 h.

For the independent LGEM evaluation with the reduced predictor set, "perfect prog" input was used for the LGEM, SHIPS, and LGEM-MR forecasts, where the predictors are determined along the best track and from GFS analyses instead of GFS forecasts. The NHC forecast track and GFS forecast could have been used (as in the real-time evaluation described in section 3), but the errors in the track and GFS model forecasts introduce errors that can mask the differences between the three models. Using predictors for the independent cases with the same level of accuracy as were used to fit the model for the dependent cases eliminates this additional source of uncertainty.

Figure 13 shows the percent improvement of the LGEM forecasts relative to LGEM-MR and SHIPS for the 2006–07 independent sample. The LGEM forecasts were better than those from SHIPS at all forecast times, with the most improvement at the longer times. The differences between SHIPS and LGEM were statistically significant at the 95% level at 72 h. LGEM showed small improvements over LGEM-MR out to 84 h, with some degradation at 96–120 h. However, none of the differences between LGEM and LGEM-MR were statistically significant, so the forecasts can be considered comparable.

The SHIPS model included 420 coefficients and LGEM-MR had 296 coefficients [14 predictors at 21 forecast times (0, 6, . . . 120 h) plus β and n]. The independent test results indicate that LGEM can produce better or comparable results with just six coefficients, which provides confidence in the generalized parameter estimation with the reduced predictor set.

8. Applications

LGEM with the reduced predictor set has a number of potential applications, which are briefly described here. Perhaps the most obvious application is for operational TC intensity forecasting, similar to what was described in section 3 for LGEM-MR. An advantage of LGEM is that there is one set of coefficients for all forecast times so that it could be used for any forecast length, provided that a track and GFS model forecast were available. This is not true for LGEM-MR because a separate set of coefficients are used at each forecast interval, and the model would have to be rederived to extend the prediction beyond 5 days. Also, given the simplicity of LGEM compared to LGEM-MR, the forecasts could be supplemented with the *S*–*C* phase diagrams and maps of the steady-state solution in (4) for interpretation of the forecasted intensities. The model could also be run along an ensemble of tracks, and with predictors from a variety of global model forecast fields. Since LGEM takes less than 1 s to run, the ensemble size could be made very large.

For operational prediction, it would be useful to incorporate persistence information in LGEM from the evolution of the storm up to the time of the forecast. As described in section 3, LGEM-MR includes persistence using the intensity changes from the previous 12 h. The generalized parameter estimation technique provides a straightforward method to incorporate any portion of the previous history up to the forecast time. For example, suppose a storm has already existed for 48 h, so that the intensity and track are known from $t = -48$ h to $t = 0$. The six LGEM constants that provided the best fit to the intensity during this period could easily be determined, as was done for the simulation of individual storm life cycles in section 6. It would also be possible to optimize the model by varying only a subset of the six constants. Then, a weighted average of the constants that best fit the previous history of the storm and those from the fit to the developmental sample could be used during the forecast period. Considerable experimentation would be required to refine this procedure, but in principle, this method could be used to incorporate any portion of the previous storm history to improve the future forecasts.

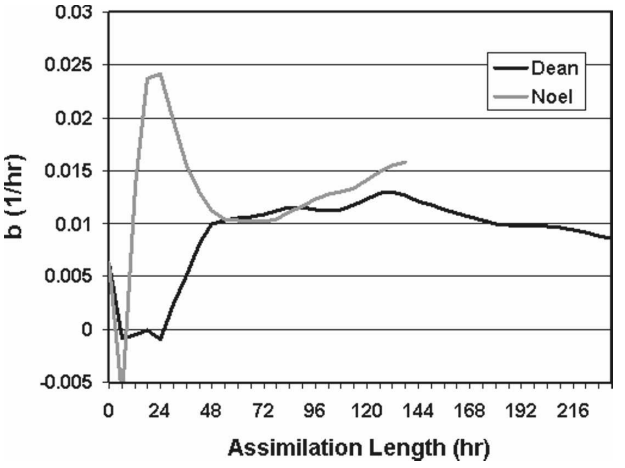

FIG. 14. The coefficient b, which represents the mean value of the growth rate κ, when fitted to the first 6 h, first 12 h, . . . , etc., of the observed intensities of Hurricanes Dean and Noel from the 2007 Atlantic hurricane season.

As a preliminary test of this idea, the two Atlantic storms from 2007 that lasted at least 5 days (Dean and Noel) were considered, and only one of the six LGEM constants [b in (25)] was allowed to vary during the preforecast fitting procedure. The value of b that optimized the 0–6, 0–12, and so on up to the full life cycle, of each storm was determined, holding the other five constants at their values from the 2001 to 2006 fit. Figure 14 shows the values of b as a function of the length of the previous history period. This figure shows that b changes fairly rapidly until about a 48-h history of the storm intensity is available. After that time, the optimal value of b becomes fairly stable. This result suggests that this procedure may only be useful after a long enough storm history is available.

NHC's guidance models, including SHIPS and LGEM-MR, are run for all existing storms. It would also be possible to combine LGEM with a global model prediction to make a genesis and intensity forecast. The GFS model includes a "tracker" (Marchok 2008) that uses automated procedures to detect the formation of tropical cyclones and then track them. Once a storm was identified in the model, LGEM could be applied to make an intensity prediction using the GFS model track and forecast fields to determine the necessary predictors.

An application related to genesis–intensity prediction is the use of LGEM as a downscaling procedure in climate simulations. Climate models develop circulations that resemble tropical cyclones, but are less intense than observed storms due to resolution limitations (e.g., Bengtsson et al. 2007). Once a procedure to identify tropical cyclones in the climate model was de-

veloped, LGEM could be applied to estimate the intensity given the SST and the atmospheric fields. For this application it would be preferable to replace the empirically based MPI formula that is a function only of SST with a more general formula such as that of Bister and Emanuel (1998), which also takes into account the atmospheric environment.

9. Concluding remarks

A simplified dynamical system for TC intensity prediction based on a logistic growth equation (LGE) was developed. The application of the LGE is based on an analogy with population dynamics, and constrains the solution to lie between zero and an upper bound. The maximum wind evolution over land is determined by an empirical inland wind decay formula and the combined water–land prediction system is referred to as the LGE model (LGEM). The LGE contains four free parameters, which are the time dependent growth rate and MPI, and two constants that determine how quickly the intensity relaxes toward the MPI. The MPI was estimated from an empirical formula as a function of SST and storm translational speed. A version of LGEM where the remaining parameters were determined by a multiple regression method using a subset of the input to the SHIPS model was run in real time in 2006–07 (called LGEM-MR). Results showed that the average LGEM-MR forecasts were up to 17% smaller than those from the SHIPS model.

LGEM-MR contains almost as many prediction coefficients as the SHIPS model (296 versus 420). The adjoint of LGEM was used to provide a more general method for finding the free parameters to make the predictions as close as possible to the NHC best-track intensities. Under the assumption that the growth rate is a function of the vertical shear (S) and a convective instability parameter (C) determined from an entraining plume model, the adjoint parameter estimation technique was used to develop a version of LGEM with just six coefficients. It was shown that this version can very accurately simulate the life cycles of individual storms when fitted to the observed intensities. For use in a predictive mode, a single set of the six coefficients was determined by fitting all Atlantic cases from the 2001–06 seasons. Results from dependent and independent cases show that the reduced predictor set version of LGEM fits the observed intensities better than the SHIPS formulation and comparable to LGEM-MR. Results also show that the LGEM solution (and some properties of real storms) can be explained by the evolution in the two-dimensional S–C phase space.

Several potential LGEM applications were described, including real-time forecasting, ensemble prediction and coupling with a global model to produce a genesis and intensity forecast. LGEM could also be used in a "downscale" mode in climate models to compensate for the lack of horizontal resolution.

This paper presented the basic framework of LGEM. There are a number of ways that the model could be improved. For real-time forecasting a procedure for including the storm intensity history up to the time of the forecast was outlined. Considerable experimentation is needed to determine the optimal way to include that information. Also, the parameters of the entraining plume model were chosen from physical considerations. These parameters could also be tuned to optimize the intensity forecasts. Finally, the surface temperature in the MPI calculation and in the entraining plume model was assumed to be equal to the SST. The current version of SHIPS includes a very simple ocean cooling parameterization based on the work of Cione and Uhlhorn (2003) that is a function of latitude and storm translational speed. It might be possible to improve LGEM by incorporating a more general cooling parameter that also includes storm intensity and subsurface ocean structure information, which is currently included in SHIPS from satellite altimetry based OHC analyses.

Acknowledgments. The author thanks Jason Dunion for the mean tropical sounding; Jim Kossin and Matt Sitkowski for their secondary eyewall formation database; and Chris Landsea, Andrea Schumacher, John Knaff, and an anonymous reviewer for their valuable comments. The views, opinions, and findings in this report are those of the author and should not be construed as an official NOAA or U. S. government position, policy, or decision.

REFERENCES

Bender, M., I. Ginis, R. Tuleya, B. Thomas, and T. Marchok, 2007: The operational GFDL coupled hurricane-ocean prediction system and a summary of its performance. *Mon. Wea. Rev.,* **135,** 3965–3989.

Bengtsson, L., K. Hodges, M. Esch, N. Keenlyside, L. Kornblueth, J.-J. Luo, and T. Yamagata, 2007: How may tropical cyclones change in a warmer climate? *Tellus,* **59A,** 539–561.

Beven, J. L., 2003: Tropical Cyclone Report, Hurrican Claudette, 8–17 July 2003. [Available online at www.nhc.noaa.gov/2003claudette.shtml.]

——, 2004: Tropical Cyclone Report, Hurricane Frances, 25 August–8 September 2004. [Available online at www.nhc.noaa.gov/2004frances.shtml.]

Bister, M., and K. A. Emanuel, 1998: Dissipative heating and hurricane intensity. *Meteor. Atmos. Phys.,* **50,** 233–240.

Cione, J. J., and E. W. Uhlhorn, 2003: Sea surface temperature

variability in hurricanes: Implications with respect to intensity change. *Mon. Wea. Rev.,* **131,** 1783–1796.

DeMaria, M., and J. Kaplan, 1994: Sea surface temperature and the maximum intensity of Atlantic tropical cyclones. *J. Climate,* **7,** 1324–1334.

——, M. Mainelli, L. K. Shay, J. A. Knaff, and J. Kaplan, 2005: Further Improvements to the Statistical Hurricane Intensity Prediction Scheme (SHIPS). *Wea. Forecasting,* **20,** 531–543.

——, J. A. Knaff, and J. Kaplan, 2006: On the decay of tropical cyclone winds crossing narrow landmasses. *J. Appl. Meteor. Climatol.,* **45,** 491–499.

——, ——, and C. R. Sampson, 2007: Evaluation of long-term trends in operational tropical cyclone intensity forecasts. *Meteor. Atmos. Phys.,* **59,** 19–28.

Emanuel, K. A., 1986: An air-sea interaction theory for tropical cyclones. Part I: Steady-state maintenance. *J. Atmos. Sci.,* **43,** 585–605.

——, 1988: The maximum intensity of hurricanes. *J. Atmos. Sci.,* **45,** 1143–1155.

——, 2000: A statistical analysis of tropical cyclone intensity. *Mon. Wea. Rev.,* **128,** 1139–1152.

——, C. DesAutels, C. Holloway, and R. Korty, 2004: Environmental controls on tropical cyclone intensity. *J. Atmos. Sci.,* **61,** 843–858.

Errico, R. M., 1997: What is an adjoint model? *Bull. Amer. Meteor. Soc.,* **78,** 2577–2591.

Franklin, J. L., and M. DeMaria, 1992: The impact of omega dropwindsondes on barotropic hurricane track forecasts. *Mon. Wea. Rev.,* **120,** 381–391.

Holland, G. J., 1997: The maximum potential intensity of tropical cyclones. *J. Atmos. Sci.,* **54,** 2519–2541.

Jarvinen, B. R., C. J. Neumann, and M. A. S. Davis, 1984: A tropical cyclone data tape for the North Atlantic Basin, 1886-1983: Contents, limitations, and uses. NOAA Tech. Memo. NWS NHC 22, NHC, Coral Gables, FL, 21 pp. [Available online at www.nhc.noaa.gov/pdf/NWS-NHC-1988-22.pdf.]

Kaplan, J., and M. DeMaria, 1995: A simple empirical model for predicting the decay of tropical cyclone winds after landfall. *J. Appl. Meteor.,* **34,** 2499–2512.

——, and ——, 2001: On the decay of tropical cyclone winds after landfall in the New England area. *J. Appl. Meteor.,* **40,** 280–286.

——, and ——, 2003: Large-scale characteristics of rapidly intensifying tropical cyclones in the North Atlantic basin. *Wea. Forecasting,* **18,** 1093–1108.

Knabb, R. D., J. R. Rhome, and D. P. Brown, 2005: Tropical Cyclone Report, Hurricane Katrina, 23–30 August 2005. NHC, 43 pp. [Available online at www.nhc.noaa.gov/pdf/TCR-AL122005_Katrina.pdf.]

Knaff, J. A., M. DeMaria, B. Sampson, and J. M. Gross, 2003: Statistical, five-day tropical cyclone intensity forecasts derived from climatology and persistence. *Wea. Forecasting,* **18,** 80–92.

——, T. A. Cram, A. B. Schumacher, J. P. Kossin, and M. DeMaria, 2008: Objective identification of annular hurricanes. *Wea. Forecasting,* **23,** 17–28.

Krishnamurti, T. N., C. M. Kishtawal, T. LaRow, D. Bachiochi, Z. Zhang, C. E. Williford, S. Gadgil, and S. Surendran, 1999: Improved skills for weather and seasonal climate forecasts from a multimodel superensemble. *Science,* **285,** 1548–1550.

LeMone, M. A., and E. J. Zipser, 1980: Cumulonimbus vertical velocity events in GATE. Part I: Diameter, intensity, and mass flux. *J. Atmos. Sci.,* **37,** 2444–2457.

Mainelli, M., M. DeMaria, L. K. Shay, and G. Goni, 2008: Application of oceanic heat content estimation to operational forecasting of recent Atlantic category 5 hurricanes. *Wea. Forecasting,* **23,** 3–16.

Marchok, T., 2008: NCEP/EMC tracking of cyclogenesis in models. [Available online at www.emc.ncep.noaa.gov/gmb/tpm/emchurr/tcgen/.]

Miller, B. I., 1958: On the maximum intensity of hurricanes. *J. Meteor.,* **15,** 184–195.

Murray, B. G., 1979: *Physiological Ecology.* Academic Press, 212 pp.

Ooyama, K. V., 1990: A thermodynamic foundation for modeling the moist atmosphere. *J. Atmos. Sci.,* **47,** 2580–2593.

Reynolds, R. W., N. A. Rayner, T. M. Smith, D. C. Stokes, and W. Wang, 2002: An improved in situ and satellite SST analysis for climate. *J. Climate,* **15,** 1609–1625.

Schwerdt, R. W., F. P. Ho, and R. R. Watkins, 1979: Meteorological criteria for standard project hurricane and probable maximum hurricane windfields, Gulf and East Coast of the United States. NOAA Tech. Rep. NWS 23, 317 pp. [Available from NWS NOAA, U.S. Department of Commerce, 8060 13th St. Silver Spring, MD 20910.]

Shen, W., 2005: A simple prediction model of hurricane intensity. *Quart. J. Roy. Meteor. Soc.,* **131,** 2887–2906.

Simpson, J., and V. Wiggert, 1969: Models of precipitating cumulus towers. *Mon. Wea. Rev.,* **97,** 471–489.

Surgi, N., R. Tuleya, Q. Lui, V. Tallapragada, and Y. Kwon, 2008: Advancement of the HWRF for the Next Generation Prediction at NCEP's Environmental Modeling Center. *Proc. 62nd Interdepartmental Hurricane Conf.,* Charleston, SC, Office of the Federal Coordinator for Meteorology, 32 pp. [Available online at http://www.ofcm.gov/ihc08/linking_file_ihc08.htm.]

Thieme, H. R., 2003: *Mathematics in Population Biology.* Princeton University Press, 543 pp.

Whitney, L. D., and J. S. Hobgood, 1997: The relationship between sea surface temperature and maximum intensities of tropical cyclones in the eastern North Pacific Ocean. *J. Climate,* **10,** 2921–2930.

Wilks, D. S., 2006: *Statistical Methods in the Atmospheric Sciences.* 2nd ed. Elsevier, 627 pp.

Yang, F., H.-L. Pan, S. K. Krueger, S. Moorthi, and S. J. Lord, 2006: Evaluation of the NCEP Global Forecast System at the ARM SGP site. *Mon. Wea. Rev.,* **134,** 3668–3690.

Zeng, Z., L. Chen, and Y. Wang, 2008: An observational study of environmental dynamical control of tropical cyclone intensity in the Atlantic. *Mon. Wea. Rev.,* **136,** 3307–3322.

Zhu, Y., and I. M. Navon, 1999: Impact of parameter estimation on the performance of the FSU global spectral model using its full-physics adjoint. *Mon. Wea. Rev.,* **127,** 1497–1517.

Zipser, E., 2003: Some views on "Hot Towers" after 50 years of tropical field programs and two years of TRMM data. *Cloud Systems, Hurricanes, and the Tropical Rainfall Measuring Mission (TRMM)–A Tribute to Dr. Joanne Simpson, Meteor. Monogr.,* No. 29, Amer. Meteor. Soc., 49–57.